

## Letter

# Chimera patterns in the Kuramoto–Battogtokh model

Lev Smirnov<sup>1,2</sup>, Grigory Osipov<sup>1</sup> and Arkady Pikovsky<sup>1,3</sup>

<sup>1</sup> Department of Control Theory, Nizhny Novgorod State University, Gagarin Av. 23, 606950, Nizhny Novgorod, Russia

<sup>2</sup> Institute of Applied Physics of the Russian Academy of Sciences, Ul'yanov str. 46, 603950, Nizhny Novgorod, Russia

<sup>3</sup> Institute for Physics and Astronomy, University of Potsdam, Karl-Liebknecht-Str. 24/25, D-14476 Potsdam-Golm, Germany

E-mail: [smirnov\\_lev@appl.sci-nnov.ru](mailto:smirnov_lev@appl.sci-nnov.ru) and [pikovsky@uni-potsdam.de](mailto:pikovsky@uni-potsdam.de)

Received 24 August 2016, revised 24 November 2016

Accepted for publication 28 December 2016

Published 16 January 2017



CrossMark

**Abstract**

Kuramoto and Battogtokh (2002 *Nonlinear Phenom. Complex Syst.* **5** 380) discovered chimera states represented by stable coexisting synchrony and asynchrony domains in a lattice of coupled oscillators. After a reformulation in terms of a local order parameter, the problem can be reduced to partial differential equations. We find uniformly rotating, spatially periodic chimera patterns as solutions of a reversible ordinary differential equation, and demonstrate a plethora of such states. In the limit of neutral coupling they reduce to analytical solutions in the form of one- and two-point chimera patterns as well as localized chimera solitons. Patterns at weakly attracting coupling are characterized by virtue of a perturbative approach. Stability analysis reveals that only the simplest chimeras with one synchronous region are stable.

Keywords: nonlocal coupled oscillators, chimera state, coarse-grained order parameter, Ott–Antonsen reduction, perturbation approach, linear stability analysis

(Some figures may appear in colour only in the online journal)

**1. Introduction**

Chimera states in populations of coupled oscillators have attracted great attention since their first observation and theoretical explanation by Kuramoto and Battogtokh [1]. The essence of chimera is in the breaking of symmetry: although a homogeneous fully symmetric synchronous state exists, yet another nontrivial state combining synchrony and asynchrony is possible

and can even be stable. Chimeras can be found during the interaction of several populations of oscillators [2–5], or in an oscillatory medium [6–9], the latter situation can be treated as a pattern formation problem. Here, formulation in terms of a coarse-grained order parameter indeed allows one to reduce the problem to that of evolution of a complex field [8, 9]. For a recent review see [10].

The goal of this paper is to develop a theory of chimera patterns in a one-dimensional (1D) medium. The main questions we address are: (i) Are complex chimera states possible? (ii) Do solitary chimera states exist in an infinite medium? (iii) Is there a way of an analytical description of chimera patterns? (iv) What are stability properties of chimera patterns? Formulation of the problem as a set of partial differential equations (PDEs) allows us to represent chimera states as solutions of ordinary differential equations (ODEs). Spatially periodic chimeras correspond to periodic orbits, of different complexity, of these ODEs. We show that in the limit of neutral coupling, these equations are integrable, yielding singular solitary ‘one-point’ and ‘two-point’ chimeras; for a weakly attracting coupling we find the properties of the chimera patterns by virtue of a perturbation analysis of these solutions. Furthermore, we study stability of the found chimera patterns by employing a numerical method allowing one to disentangle essential continuous and discrete (point) parts [11, 12] of the stability spectrum.

## 2. Formulation of the problem

The original Kuramoto–Battogtokh (KB) model [1] is formulated as a 1D field of phase oscillators  $\phi(x, t)$  evolving according to

$$\partial_t \phi = \omega + \text{Im} \left[ \exp(-i\phi(x, t) - i\alpha) \int G(x - \tilde{x}) \exp(i\phi(\tilde{x}, t)) d\tilde{x} \right], \quad (1)$$

with the exponential kernel  $G(y) = \kappa \exp(-\kappa|y|)/2$ . The coupling is attractive if the phase shift  $\alpha < \pi/2$ , then the synchronous state where all the phases are equal is stable;  $\alpha = \pi/2$  corresponds to neutral coupling.

One can reformulate this setup as a continuous oscillatory medium [8, 9] described by the complex field  $Z(x, t)$ , which represents a coarse-grained order parameter of the phases:  $Z(x, t) = \lim_{\delta \rightarrow 0} \frac{1}{2\delta} \int_{x-\delta}^{x+\delta} \exp[i\phi(\tilde{x}, t)] d\tilde{x}$ . In the synchronous state  $|Z| = 1$ , while for partial synchrony,  $0 < |Z| < 1$ . The dynamics of  $Z(x, t)$  just follows locally the Ott–Antonsen equation [10, 13]

$$\partial_t Z = i\omega Z + (e^{-i\alpha} H - e^{i\alpha} H^* Z^2)/2. \quad (2)$$

Here the field  $H(x, t) = \int G(x - \tilde{x}) Z(\tilde{x}, t) d\tilde{x}$  describes the force due to coupling. This nonlocal coupling stems from the following model for the interaction of oscillators via the ‘auxiliary’ field  $H(x, t)$  (see [7, 14, 15]):

$$\tau \partial_t H = \kappa^{-2} \partial_{xx}^2 H - H + Z. \quad (3)$$

Parameter  $\tau$  indicates the characteristic time scale of the function  $H(x, t)$ . In the limit of the infinitely fast dynamics of the auxiliary field, where  $\tau \rightarrow 0$ , (3) reduces to an equation

$$\partial_{xx}^2 H - \kappa^2 H = -\kappa^2 Z, \quad (4)$$

the solution of which depends on boundary conditions. In particular, in an infinite medium  $|x| < \infty$ , the solution is  $H(x, t) = \int [\kappa \exp(-\kappa|x - \tilde{x}|)/2] Z(\tilde{x}, t) d\tilde{x}$  as in (1).

Below we consider a spatially periodic medium with period  $L$ ; in this case, the KB model exactly corresponds to (2) and (4) if the integration is performed in the infinite domain, while the fields are assumed to have a period  $L$ . If the integration over the periodic domain of size  $L$  is performed, one should use the kernel

$$G(y) = \frac{\kappa}{2 \sinh(\kappa L/2)} \cosh[\kappa(|y| - L/2)], \quad (5)$$

which follows from the solution of (4) with periodic boundary conditions. Specifically, the kernel (5) is the Green's function of the inhomogeneous Helmholtz equation with the source on the right-hand side and corresponding conditions at the points  $x = 0$  and  $x = L$ . This form of  $G(y)$  allows transforming from the integro-differential equation (2) with a temporary instantaneous, integral relation between  $Z(x, t)$  and  $H(x, t)$  to the system of PDEs (2) and (4). Similar technique was also applied earlier in neural field theory [16] and spatially extended networks of coupled oscillators [14, 15]. In particular, in [15] the basic chimera state (case A in figure 1) has been found as a solution of a complex ODE, however more general solutions have not been discussed there. Noteworthy, our method does not work for other kernels studied in this context, e.g. for a popular piece-wise constant kernel.

The formulated problem (2) and (4) contains two parameters having the length dimension  $L$  and  $\kappa^{-1}$ . By rescaling the coordinate  $x$ , we can set one of these parameters to one. It is convenient to set  $\kappa = 1$ , then the only parameter is the size of the system  $L$ .

### 3. Chimera states as solutions of ODE

Our next goal is to find chimera states, which consist of synchronous and asynchronous parts. We look for the rotating-wave solutions of system (2) and (4), which are stationary in a rotating reference frame:  $Z(x, t) = z(x) \exp[i(\omega + \Omega)t]$ ,  $H(x, t) = h(x) \exp[i(\omega + \Omega)t]$ , where  $\Omega$  is some unknown frequency to be defined below<sup>4</sup>. Substituting this, we get a system of an algebraic equation and an ODE for complex functions  $z(x)$  and  $h(x)$ :

$$e^{i\alpha} h^* z^2 + 2i \Omega z - e^{-i\alpha} h = 0, \quad (6)$$

$$h'' - h = -z. \quad (7)$$

Here and below, primes denote spatial derivatives.

The first step is to express  $z(x)$  from the quadratic equation (6). This equation describes the order parameter  $z(x)$  of a set of oscillators driven by the field  $h(x) = r(x) \exp[i\theta(x)]$ , the solution at each point  $x$  depends on the relation between  $r$  and  $\Omega$  (below, for simplicity of presentation, we write the relations for  $\Omega < 0$ ). If  $|r| \geq |\Omega|$ , then the oscillators are locked and  $|z| = 1$ , otherwise the oscillators are partially synchronous with  $0 < |z| < 1$ . The solution reads<sup>5</sup>

$$z = \begin{cases} -\left(i \Omega - \sqrt{r^2 - \Omega^2}\right) r^{-1} \exp[i(\theta - \alpha)], & \text{if } |r| \geq |\Omega|, \\ -i \left(\Omega + \sqrt{\Omega^2 - r^2}\right) r^{-1} \exp[i(\theta - \alpha)], & \text{if } |r| < |\Omega|. \end{cases} \quad (8)$$

<sup>4</sup> Here our definition of the frequency  $\Omega$  is the same as in the KB paper [1]. This frequency will be negative, if  $\alpha \lesssim \pi/2$ .

<sup>5</sup> In order to make the coupling between  $z(x)$  and  $h(x)$  unique, it is needed to select one of the two solutions of the quadratic equation (6). This can easily be done based on the physical meaning of the local order parameter  $Z(x, t)$  and taking into account that the amplitude of  $Z(x, t)$  cannot be greater than unity, i.e.  $|Z(x, t)| \leq 1$  (see, e.g. [8, 11, 17]). If there are two solutions with  $|Z(x, t)| < 1$ , the locally stable one is chosen.

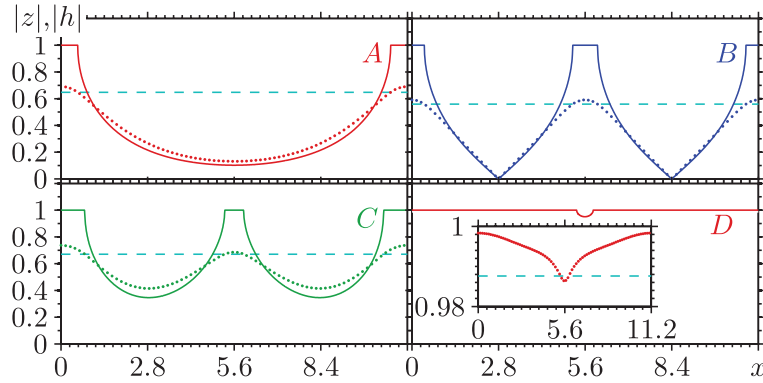


**Figure 1.** Profiles of the simplest chimeras (with at most two SRs) for  $\alpha = 1.457$ ,  $|z|$ : solid lines,  $|h|$ : dotted lines. *A*: the KB one-SR chimera for  $\Omega = -0.648$ , *B*: symmetric two-SRs chimera for  $\Omega = -0.558$ , *C*: asymmetric two-SRs chimera (here, the sizes of the synchronous domains are different, and their phases differ not by  $\pi$ , unlike in case *B*) for  $\Omega = -0.672$ , *D*: nearly synchronous one-SR chimera for  $\Omega = -0.98762$ . The colors correspond to coding of the solutions in figure 4.

We substitute this solution in (7). Although  $h(x)$  is complex, the resulting equation can be written, due to gauge invariance  $\theta(x) \rightarrow \theta(x) + \theta_0$ , as a third-order system of ODEs for the real functions  $r(x)$  and  $q(x) = r^2(x)\theta'(x)$

$$\begin{aligned} r'' &= r + r^{-3}q^2 - r^{-1}\sqrt{r^2 - \Omega^2} \cos \alpha + r^{-1}\Omega \sin \alpha, \\ q' &= \Omega \cos \alpha + \sqrt{r^2 - \Omega^2} \sin \alpha, \end{aligned} \quad (9)$$

in the domain where  $|r| \geq |\Omega|$ , and

$$\begin{aligned} r'' &= r + r^{-3}q^2 + r^{-1}\left(\Omega + \sqrt{\Omega^2 - r^2}\right) \sin \alpha, \\ q' &= \left(\Omega + \sqrt{\Omega^2 - r^2}\right) \cos \alpha, \end{aligned} \quad (10)$$

in the domain where  $|r| < |\Omega|$ . We note here that the right-hand side of (9) and (10) are not Lipschitz continuous at  $r = \Omega$ . However, the uniqueness of solutions is not violated because there are no solutions tangent to the set  $r = \Omega$ .

Our goal is to find chimera patterns described by (9) and (10) satisfying the periodicity condition  $r(x + L) = r(x)$ ,  $q(x + L) = q(x)$ . It is more convenient not to fix the period  $L$ , but to fix the frequency of the rotating chimera  $\Omega$  and then find periodic solutions of (9) and (10); period  $L$  of which depends on  $\Omega$ . This will after the inversion yield dependence  $\Omega(L)$ .

Before discussing numerical and analytical approaches, we illustrate in figure 1 several solutions for  $\alpha = 1.457$  (the value used in [1]) with period  $L \approx 11.2$ . The presented solutions (types *A* and *B* have been already discussed in the literature [1, 10, 12]) are just the simplest possible chimeras with at most two synchronous regions (SRs). Indeed, the system (9) and (10) is a reversible (with respect to involution  $r \rightarrow r$ ,  $q \rightarrow -q$ ) third-order system of ODEs with a plethora of solutions, including chaotic ones. We illustrate this by constructing a two-dimensional Poincaré map in figure 2(a).

Starting with an initial condition satisfying  $r'(0) = 0$  and  $q(0) = 0$ , we integrate, for various values  $r(0)$ , the system (9) and (10) and selected all points with  $r' = 0$  and  $r'' < 0$  (i.e.

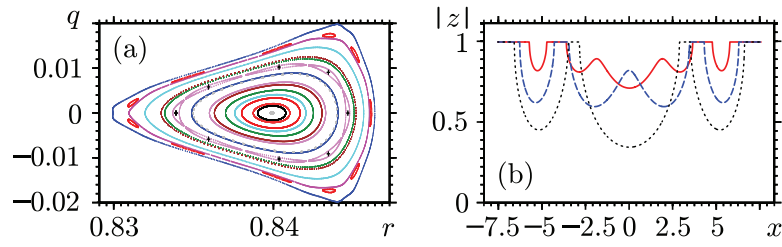


**Figure 2.** (a) Poincaré map for system (9) and (10) for  $\alpha = 1.457$  and  $\Omega = -0.8$ . The condition for the section:  $r' = 0, r'' < 0$ . (b) More complex patterns with three SRs for  $L \approx 15.1$  and  $\Omega = -0.796$  (solid red line),  $\Omega = -0.726$  (dashed blue line) and  $\Omega = -0.674$  (dotted black line).

maxima of the profile  $r(x)$ ). The Poincaré map is accomplished by plotting the resulting points on the plane  $(r, q)$ . One can see in figure 2(a) different trajectories: fixed points and periodic orbits that correspond to periodic trajectories of the original system of ODEs; closed invariant curves corresponding to quasiperiodic solutions. This is a typical picture of tori and periodic orbits of different periods for nearly integrable Hamiltonian systems. Not all points on the Poincaré surface lead to physically meaningful solutions: we discard the trajectories which resulted in values  $|r| > 1$ . The fixed point of the map figure 2(a) at  $q = 0, r \approx 0.84$  describes the one-hump chimera state A in figure 1. The periodic orbit marked with crosses in figure 2(a) corresponds to a periodic in space profile having eight maxima of  $r(x)$ . Closed invariant curves describe possible quasiperiodic in space states in an infinite medium.

The Poincaré map figure 2(a) is constructed for a fixed value of  $\Omega$ . It provides several branches of periodic orbits having different periods. Collecting solutions at a fixed period  $L$  (which do not correspond to one Poincaré map, but rather to different maps at different values of  $\Omega$ ), we obtain many coexisting chimera patterns; several three-SRs chimeras are illustrated in figure 2(b). Chimera states with multiple synchronous and asynchronous parts were already reported in some other papers (see, e.g. [17–19]). Similar complex patterns appear also in other physical setups (e.g. multi-peak solitons in nonlinear optics), a special feature of chimera patterns is that they are non-smooth in terms of the order parameter  $|z|$  and look like sharp zebra stripes ‘order-disorder’ [19]. Our aim in this study is not to follow all possible periodic and chaotic solutions of this reversible system. Below we focus on the simplest ones illustrated in figure 1 corresponding to fixed points and period-two orbits of the Poincaré map.

#### 4. Analytical approach for chimera states. One- and two-point chimeras

Remarkably, it is possible to describe basic chimera profiles semi-analytically, for  $\alpha \approx \pi/2$ . Let us first consider the limiting case  $\alpha = \pi/2$ . Here, according to (9) and (10), the derivative  $q'(x)$  is non-negative in the synchronous state and vanishes in the asynchronous state. Thus, a periodic solution with  $q(x) = q(x + L)$  should be at all points asynchronous, possibly except for one or two points at which  $r(x)$  achieves an extremum  $|r| = |\Omega|$ . For this degenerate chimera, (10) reduce to  $q = 0$ <sup>6</sup> and an integrable second-order equation

<sup>6</sup>The case  $\alpha = \pi/2$  implies  $q'(x) = 0$  for the asynchronous regime, leading to the constant product  $r^2(x)\theta'(x) = q_0$ . Therefore,  $\theta'(x) = q_0/r^2(x)$  is a fixed-sign value. From the condition of periodicity for  $h(x)$  at an interval  $[0, L)$ , it follows that  $\theta(x + L) - \theta(x) = 2\pi s$ , where  $s$  is integer, which is obviously satisfied in particular at  $q(x) = q_0 = 0$ . Physically, setting  $q_0 = 0$ , we discuss only cases where the drift along the spatial coordinate  $x$  is absent in the steady motion of the phase oscillators.

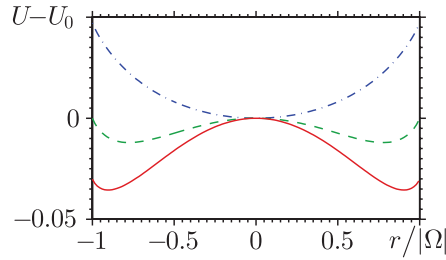


**Figure 3.** Potential  $U(r)$  for  $\Omega = -0.3$  (dash-dotted blue curve),  $\Omega = \Omega_*$  (dashed green curve),  $\Omega = -0.7$  (solid red curve). Here  $U_0 = -\Omega \ln(2|\Omega|) - |\Omega|$ .

$$r'' = -dU(r)/dr, \tag{11}$$

$$U(r) = -r^2/2 - \sqrt{\Omega^2 - r^2} - \Omega \ln\left(\sqrt{\Omega^2 - r^2} - \Omega\right). \tag{12}$$

In the potential  $U(r)$  shown in figure 3 for three different values of  $\Omega$ , there are two types of trajectories having the maximum at  $r_{\max} = |\Omega|$ , depending on the value of  $\Omega$ . For  $-1 < \Omega < \Omega_* = 2(\ln 2 - 1)$  this is a periodic orbit with  $0 < r_{\min} \leq |\Omega|$ . It reaches the boundary of the asynchronous region at one point and corresponds to a ‘one-point chimera’, which can be considered as the limiting case of curve  $A$  in figure 1, where the SR shrinks to a point. For  $\Omega_* < \Omega < 0$  there is a symmetric periodic orbit (here, it is convenient to allow  $r$  to change sign; this corresponds to a jump by  $\pi$  in  $\theta$  if  $r$  is considered positive as in figure 1, curve  $B$ ) with  $-|\Omega| \leq r \leq |\Omega|$ . This ‘two-point chimera’ corresponds to curve  $B$  in figure 1. These two types of solutions merge in a homoclinic orbit with infinite period at  $\Omega = \Omega_*$ , which can be named ‘chimera soliton’ (one- or two-point, depending on which side of the threshold the orbit is considered). Physically, chimera solitons correspond to localized states of enhanced synchrony in an infinite medium, with full synchrony (maximal order parameter  $|z| = 1$ ) being achieved just at one point. The dependencies  $\Omega(L)$  for these solutions are shown in figure 4 as solid lines. Note that additionally there is a branch of synchronous solutions with  $\Omega = -1$  which are steady states  $r = 1$ .

The solutions above are degenerate chimeras, as the SR is restricted to one or two points. The SR becomes finite for  $\alpha \lesssim \pi/2$ , here one can develop a perturbation approach by introducing a small parameter  $\beta = \pi/2 - \alpha \ll 1$ . Now  $q \neq 0$ , but because  $q \sim \beta$ , we can neglect terms  $\sim q^2$  in (9) and (10). Then, the problem reduces to finding a periodic trajectory  $r(x)$  of the integrable equation, such that the evolution of  $q(x)$  is periodic:

$$\oint q'(x) dx = \int_{x: |r(x)| \geq |\Omega|} \left( \Omega \beta + \sqrt{r^2(x) - \Omega^2} \right) dx + \int_{x: |r(x)| \leq |\Omega|} \beta \left( \Omega + \sqrt{\Omega^2 - r^2(x)} \right) dx = 0. \tag{13}$$

The result is that the size  $L_{\text{syn}}$  of SR becomes finite:

$$L_{\text{syn}}^2 \approx \frac{8\beta}{\pi N_{\text{SR}} \sqrt{|\Omega|(1-|\Omega|)}} \oint (R'^2 + R^2) dx. \tag{14}$$

where  $R(x)$  is the solution of (12) at  $\beta = 0$  and  $N_{\text{SR}}$  is the number of SRs and can take two integer values 1 or 2. Physically, the constructed solutions are long-periodic inhomogeneous

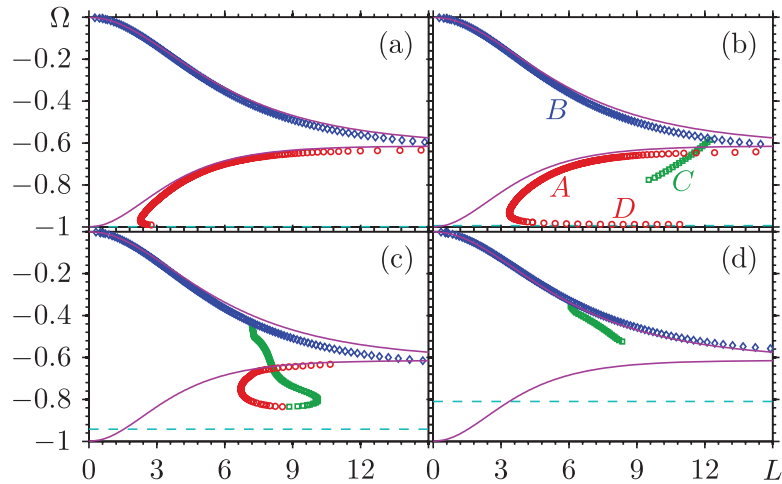


**Figure 4.** Parameter  $\Omega$  versus periods of chimera states  $L$  for  $\alpha = 1.514$  (a),  $\alpha = 1.457$  (b),  $\alpha = 1.229$  (c), and  $\alpha = 0.944$  (d). Chimera states for  $\alpha = \pi/2$ , obtained by integration (12), are shown with violet solid lines. Different markers correspond to the chimera types depicted in figure 1, as specified in panel (b). Cyan dashed lines show the frequency of the synchronous state  $\Omega = -\sin \alpha$ .

states, where oscillators are desynchronized almost everywhere, except for one or two small regions of enhanced coherence, which is full in smaller core zones.

We compare the analytical approach above with the results of direct numerical calculations (within the framework of (9) and (10)) of periodic orbits in figure 4, for several values of  $\alpha$ . Panel (a) shows that for small  $\beta$  chimera states (of types *A* and *B* in figure 1) are close to degenerate regimes at  $\beta = 0$ . One can see in panels (a) and (b) that the two analytic solutions at  $\alpha = \pi/2$  (the one-point chimera and the synchronous state) merge into one branch at  $\alpha \lesssim \pi/2$  with a nonmonotonous dependence  $\Omega$  on  $L$ , see one-SR chimeras *A* and *D* in figure 1. In panel (b) one can see an additional branch corresponding to the two-SRs asymmetric chimera *C* in figure 1. As a result, in (b) and (c) one has four solutions in some range of periods  $L$ . Only two of them survive for small  $\alpha$ ; diagrams for  $\alpha < 0.9$  are qualitatively the same as panel (d) in figure 4.

### 5. Stability analysis

Next, we discuss stability of the obtained chimera patterns. For this goal we linearize (2) and (5). Contrary to the problem of finding chimera solutions, this analysis cannot be reduced to that of differential equations, rather we have to consider the integro-differential equations (2) and (5) for  $Z(x, t)$ . After spatial discretization, we get a matrix eigenvalue problem. The difficulty here is that, according to [12, 17], there is an essential continuous *T*-shaped spectrum  $\lambda_c$  consisting of eigenvalues on the imaginary and the negative real axes, but stability is determined by the point spectrum  $\lambda_p$ . Unfortunately, it is not easy to discriminate these parts of the spectrum in the eigenvalues  $\lambda$  of the approximate matrix, because the eigenvalues representing the essential part of spectrum lie not exactly on the imaginary axis. We adopted the following procedure to select the point spectrum  $\lambda_p$ . For a chimera state in the domain  $0 \leq x \leq L$ , we can discretize the linearized system by using a set of points  $x_0 + j\Delta$ ,  $j = 0, 1, \dots, M - 1$ , where  $\Delta = L/M$  and  $0 \leq x_0 \leq \Delta$  is an arbitrary continuous parameter. This leads to an  $2M \times 2M$  real

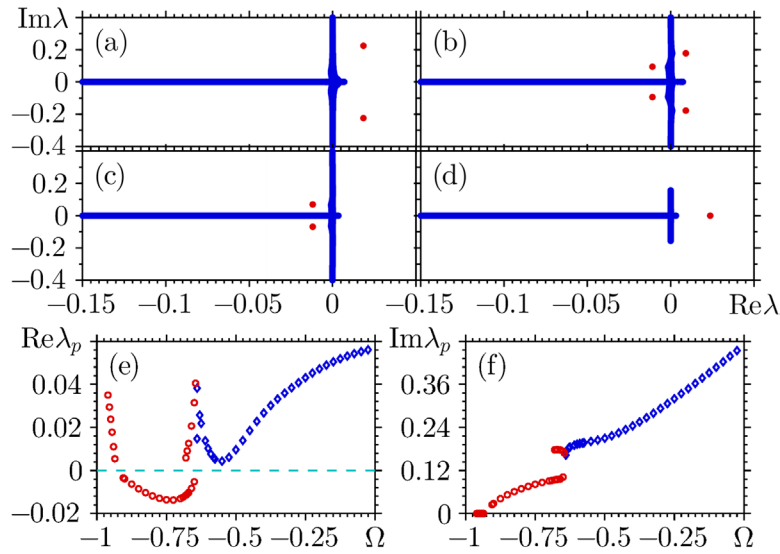


**Figure 5.** ((a)–(d)): Essential (blue markers) and point (red markers) spectra for chimera states at  $\alpha = 1.457$  and four values of  $\Omega$ : (a)  $\Omega = 0.45$ , (b)  $\Omega = 0.675$ , (c)  $\Omega = 0.8$ , (d)  $\Omega = 0.95$ . In these diagrams, all  $2MN$  eigenvalues with  $M = 2048$  and  $N = 128$  are plotted. ((e), (f)): Real and imaginary parts of the point spectrum  $\lambda_p$  for solutions  $A, D$  (red circles) and  $B$  (blue diamonds) in figure 4(b).

matrix, the eigenvalues  $\lambda$  of which we obtained numerically. Additionally, we vary the offset of the discretization  $x_0$ . In numerics we use  $M = 2048$  and  $N = 64$  or  $N = 128$  equidistant values of  $x_0$ . We find that while the components of the essential spectrum vary with  $x_0$ , the point spectrum  $\lambda_p$  components vary extremely weakly with  $x_0$ . This allows us to determine the point spectrum  $\lambda_p$  reliably for most values of the parameters.

Below we present a stability analysis for  $\alpha = 1.457$ , for branches  $A, B, C, D$  (see figure 4(b)). Four characteristic types of spectra are shown in figures 5(a)–(d). Only case (c) where the point spectrum  $\lambda_p$  has a negative real part corresponds to a stable chimera pattern, while all other patterns are unstable (oscillatory instability for cases (a) and (b) and monotonous instability for case (d)). The dependence of the point spectrum  $\lambda_p$  on parameter  $\Omega$  for  $\alpha = 1.457$ , for branches  $A, B, D$ , is shown in figures 5(e) and (f). One can see that in the region  $-0.68 \lesssim \Omega \lesssim -0.64$  there are four points of  $\lambda_p$ ; for other values of  $\Omega$ , there is only one pair of eigenvalues (or one real eigenvalue for branch  $D$ ). This property may be attributed to the fact that close to the homoclinic orbit  $\Omega \approx \Omega_*$  the length of the patterns is large, so two discrete modes are possible here. The only stable chimera state is of type  $A$  (we refer here to figures 1 and 4(b)) with  $-0.91 \lesssim \Omega \lesssim -0.69$ <sup>7</sup>. On the contrary, chimera states with two SRs (type  $B$ ) are unstable. Most difficult was the analysis of the two-SRs solutions of type  $C$  (figure 6), here the unstable branch of the point spectrum  $\lambda_p$  is real, and there are up to three stable complex pairs. In some cases, only very fine discretization with  $M = 6144$  allows us to reveal unstable point eigenvalues  $\lambda_p$ . We attribute this to a complex profile of this solution, requiring a high resolution of perturbations.

Stability properties are confirmed by direct numerical simulations of the ensemble governed by (1) and (5), see figure 7 for space-time plots of field  $|H(k, t)| = \left| \sum_j G(|k - j|/KL) \exp(i\phi_j) \right|$ .

<sup>7</sup>This agrees with an empirical observation, that ‘all multiheaded chimera states ... are of transient type with life time not exceeding several thousand time units’ (see [19] for details).

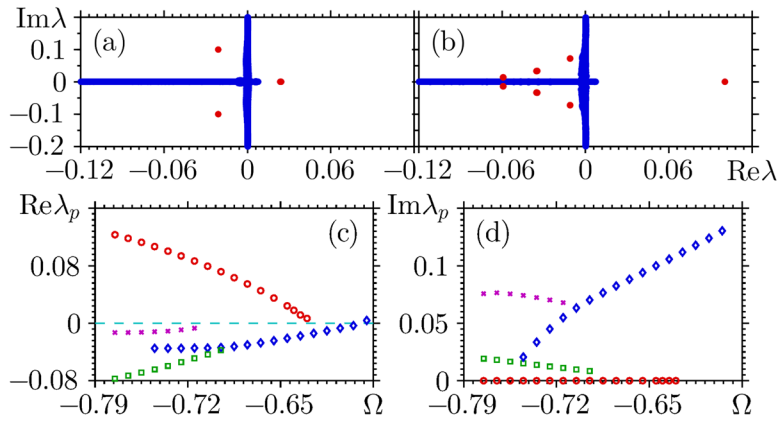


**Figure 6.** All eigenvalues ((a):  $\Omega = -0.645$ , (b):  $\Omega = -0.735$ , here  $M = 4096$ ,  $N = 64$ ) and point spectra in dependence on  $\Omega$  ((c), (d)) for the asymmetric branch C.

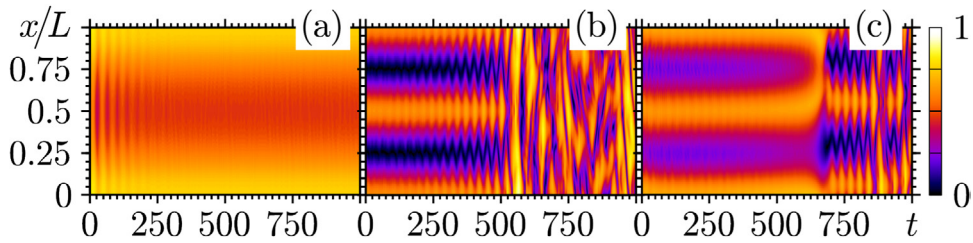


**Figure 7.** Direct numerical simulations of stable and unstable chimera for  $\alpha = 1.457$ . (a): Chimera of type A for  $\Omega = -0.71377$ ,  $L = 6.03$ ; (b): chimera of type B for  $\Omega = -0.575$ ,  $L = 12.06$ ; (c): chimera of type C,  $\Omega = -0.6$ ,  $L = 12.06$ . The number of oscillators was  $K = 700$  per length unit.

We initialize the chimera patterns found above; in the unstable regions these patterns are eventually destroyed, while a stable chimera persists. Remarkably, for weakly unstable two-SRs chimera for  $\Omega \approx -0.58$ , where the real part of the point eigenvalue  $\lambda_p$  has a minimum (see figure 5(e)), the life time of prepared chimera is relatively large.

## 6. Conclusion

Summarizing, in this letter we reformulated the problem of chimera patterns in a 1D medium of coupled oscillators as a system of PDEs. This allow us to find uniformly rotating chimera states as solutions of an ODE. We demonstrated a variety of patterns with large spatial periods, but restricted our attention in this letter to the simplest ones, with at most two synchronous domains. Remarkably, these profiles can be analytically described in the limit of neutral coupling between oscillators. For a coupling close to the neutral one, we develop a perturbation analysis which yields approximate solutions. Exploring the stability of the found solutions appears to be a non-trivial numerical problem. We suggest an approach to characterize the essential and the point parts of the spectrum via finite discretizations. It appears that only chimeras of the type originally studied by Kuramoto and Battogtokh are stable, while others are linearly unstable.

The approach above could be extended in several directions. First, one can study general bifurcations of chimera patterns. The difficulty here is that many tools for the bifurcation

analysis require sufficient smoothness of the equations, but this is not the case for chimera solutions. Stability analysis in this letter is limited to perturbations with the same spatial period as the chimera itself, i.e. it describes stability for a medium on a circle. Other unstable modes, e.g. of modulational instability type, could appear if one formulates the stability problem for an infinite medium. Finally, the formulated PDEs have been simplified using the separation of time scales; it would be interesting to study stability of chimeras in (2) and (3) with  $\tau \neq 0$ .

## Acknowledgments

We acknowledge discussions with O Omelchenko, M Wolfrum, and Yu Maistrenko. LS was supported by ITN COSMOS (funded by the European Union's Horizon 2020 research and innovation programme under the Marie Skłodowska-Curie grant agreement No 642563). Numerical part of this work was supported by the Russian Science Foundation (Project No. 14-12-00811). GO was supported by the Ministry of Education and Science of the Russian Federation (Research Assignment No. 1.115.2014/K).

## References

- [1] Kuramoto Y and Battogtokh D 2002 *Nonlinear Phenom. Complex Syst* **5** 380
- [2] Abrams D M, Mirollo R, Strogatz S H and Wiley D A 2008 *Phys. Rev. Lett.* **101** 084103
- [3] Pikovsky A and Rosenblum M 2008 *Phys. Rev. Lett.* **101** 264103
- [4] Tinsley M R, Nkomo S and Showalter K 2012 *Nat. Phys.* **8** 662
- [5] Martens E A, Thutupalli S, Fourrière A and Hallatschek O 2013 *Proc. Natl Acad. Sci* **110** 10563
- [6] Abrams D M and Strogatz S H 2004 *Phys. Rev. Lett.* **93** 174102
- [7] Shima S-I and Kuramoto Y 2004 *Phys. Rev. E* **69** 036213
- [8] Laing C R 2009 *Phys. D: Nonlinear Phenom.* **238** 1569
- [9] Bordyugov G, Pikovsky A and Rosenblum M 2010 *Phys. Rev. E* **82** 035205
- [10] Panaggio M J and Abrams D M 2015 *Nonlinearity* **28** R67
- [11] Wolfrum M, Omel'chenko O E, Yanchuk S and Maistrenko Y L 2011 *Chaos* **21** 013112
- [12] Omel'chenko O E 2013 *Nonlinearity* **26** 2469
- [13] Ott E and Antonsen T M 2008 *Chaos* **18** 037113
- [14] Laing C R 2011 *Phys. D: Nonlinear Phenom.* **240** 1960
- [15] Laing C R 2015 *Phys. Rev. E* **92** 050904
- [16] Laing C R and Troy W C 2003 *SIAM J. Appl. Dyn. Syst.* **2** 487
- [17] Xie J, Knobloch E and Kao H-C 2014 *Phys. Rev. E* **90** 022919
- [18] Sethia G C, Sen A and Johnston G L 2013 *Phys. Rev. E* **88** 042917
- [19] Maistrenko Y L, Vasylenko A, Sudakov O, Levchenko L and Maistrenko V L 2014 *Int. J. Bifurcation Chaos* **90** 1440014